International Journal for Housing Science and Its Applications
Publish August 10, 2025. Volume 46, Issue 4 Pages 8397-8412

https://doi.org/10.70517/ijhsa464715

Research on green concrete using oil palm shell aggregate based on LSSVR

Jinshuai Lu[1], Hongchang Liu[1], Shuai Cai[1] and Wenying You[1,*]
[1] Weifang Engineering Vocational College, Qingzhou, Shandong, 262500, China
Corresponding authors: (e-mail: ywy0536@163.com).

Abstract Traditional concrete currently struggles to meet the demands of the construction industry. To address this issue, oil palm shell aggregate green concrete has been developed. Raw materials for preparing oil palm shell aggregate green concrete were selected, and under the guidance of appropriate material mix ratios and preparation processes, five different samples of oil palm shell aggregate green concrete were ultimately produced. The DE-GWO combined optimization algorithm was used to optimize the least squares support vector regression model, resulting in a DE-GWO-LSSVR-based performance prediction model for oil palm shell aggregate green concrete. This model was then applied to conduct predictive empirical analysis of the performance characteristics of oil palm shell aggregate green concrete. The predictive empirical analysis revealed that the actual compressive strength test values of the 14-day samples were distributed within the range of [60.42 MPa, 62.72 MPa], with an error of less than 1 MPa compared to the target results [60.36 MPa, 63.33 MPa], which is within an acceptable range. This demonstrates the application value of the DE-GWO-LSSVR model in oil palm shell aggregate green concrete.

Index Terms LSSVR, DE, GWO, concrete

I. Introduction

Since its introduction into engineering construction, concrete has held an extremely important position in modern architecture. It plays an irreplaceable role and functions in the field of civil engineering that no other material can match. For a considerable period of time to come, cement concrete will remain the most widely used and highest-volume building material. However, the extensive use of concrete has also brought about numerous negative impacts, such as environmental issues, among others [1]-[3]. Therefore, whether concrete can continue to serve as the primary structural building material in the long term hinges on its ability to become a green material [4], [5].

Green concrete is a building material primarily composed of renewable materials and environmentally friendly components. Due to its environmental friendliness and sustainability, it has garnered increasing attention and research [6]. In the construction field, green concrete can be used to produce green wall materials, insulation materials, and earthquake-resistant materials, enhancing the energy efficiency and disaster resistance of buildings. It can also be applied in infrastructure projects such as urban roads, bridges, and tunnels, improving their durability and reducing maintenance costs [7]-[10]. Additionally, green concrete plays a significant role in water treatment, environmental restoration, and waste management [11], [12].

Research on green concrete has achieved certain results. In terms of raw materials, researchers have replaced traditional cement and aggregates with waste materials and recycled resources, such as fly ash, slag powder, and waste concrete, not only reducing dependence on limited resources but also minimizing environmental pollution [13]-[15]. Additionally, researchers have optimized the mechanical properties and durability of green concrete by adjusting its mix proportions and additives, thereby enhancing its engineering application value [16]. For example, in Reference [17], 2.5% waste polyester material, 15% natural zeolite, 1.0% waste polyester material, and ordinary Portland cement were used to replace cement concrete, resulting in green concrete with higher compressive strength and lower cost. Reference [18] used fly ash, nano-titanium dioxide, nano-calcium carbonate, sodium nitrite, and ordinary Portland cement materials in a weight ratio of 40%, 2%, 2%, 2%, and 56%, respectively, to produce high-performance green concrete with higher strength, durability, and resistance to chloride ion penetration. In Reference [19], ultra-fine palm oil fuel ash and crushed recycled plastic bottles were added to high-performance concrete, replacing the total cementitious materials and reinforcing fibers, respectively, to improve the concrete's engineering and transport properties. The addition ratio of ultra-fine palm oil fuel ash exhibited different performance characteristics at different stages.

Oil palm trees are one of the most important economic crops, but due to the lack of effective processing methods, oil palm waste has become a source of environmental pollution and health risks in many areas [20], [21]. Among

these, oil palm shell waste accounts for the largest proportion. This waste can be used as an energy source through various energy conversion methods such as pyrolysis and combustion; however, the utilization rate of oil palm shell waste is less than 30%, while its annual production remains high [22]-[24]. Therefore, concrete using oil palm shells as aggregate has garnered attention. Reference [25] investigated the optimal proportion of oil palm shells as a substitute for coarse aggregate in concrete, with an experimental gradient of 0-100% showing that 60% is the optimal ratio. Reference [26] concluded that compared to traditional aggregate concrete, oil palm shell aggregate concrete has better thermal insulation properties and density, with 28-day test data showing its compressive strength exceeds 17 N/mm². Literature [27] and [28] optimized oil palm shell aggregate concrete to further enhance its performance. By treating the surface of oil palm shell aggregate concrete with lime, the mechanical properties were improved, and adding steel fibers to 80% oil palm shell concrete increased its strength. Reference [29] found that adding fly ash to oil palm shell aggregate concrete reduces its strength and porosity as the fly ash content increases. Increasing numbers of researchers are dedicated to developing high-performance green concrete using oil palm shell aggregate. However, due to the complex performance characteristics of oil palm shell aggregate green concrete, it is difficult to predict its performance after production. Under the development of intelligent technology, this performance prediction has been studied [30], [31].

Least Squares Support Vector Regression (LSSVR) is a statistical learning method combining Support Vector Machines (SVM) with the least squares method, aimed at solving prediction problems. While inheriting the advantages of SVM, it replaces the L2 norm of the error with the insensitive loss function of SVM and uses equality constraints instead of inequality constraints, thereby transforming the convex quadratic programming problem of solving SVM into a linear equation system problem, thereby reducing algorithm complexity [32]-[34]. Reference [35] reports that the LSSVR model coupled with simulated return support can be used to explore the nonlinear relationship between concrete compressive strength and related input factors, and to predict the compressive strength of high-performance concrete. Reference [36] utilizes an LSSVR model based on the Lévy walk and beetle antenna search algorithms to predict the bond strength between fiber-reinforced polymers and concrete, providing decision-making references for structural engineering. Reference [37] compared the application of three models for predicting the mechanical properties of recycled aggregate concrete, where the LSSVR model not only performed best in predicting compressive strength but also in predicting flexural strength. Reference [38] used a sparse LSSVR method for three-dimensional localization of acoustic emission sources to locate concrete damage positions, thereby improving the accuracy of damage localization based on acoustic emission sources. Literature [39] applied the LSSVR algorithm adjusted by the ground squirrel optimization algorithm and the balanced optimization algorithm to predict the volume expansion of the paste in cement concrete containing fly ash and magnesium oxide expansive agent, thereby adjusting the concrete structure to enhance its durability and stability.

This paper is based on the theoretical knowledge of the preparation process for green concrete using oil palm shell aggregate. The composition materials and mix proportions for green concrete using oil palm shell aggregate were determined, and five samples of green concrete using oil palm shell aggregate were prepared under the guidance of the preparation process. These samples were named CTRL, POFA25, POFA50, POFA75, and POFA50-2. To investigate the performance of the five oil palm shell aggregate green concrete samples, a least squares support vector regression model was first used to predict their performance, but the results did not meet the research standards. Therefore, the DE-GWO combined optimization algorithm was applied to optimize the aforementioned model, ultimately designing a performance prediction model for oil palm shell aggregate green concrete based on DE-GWO-LSSVR. Based on the research data, the application effectiveness of the model was empirically analyzed from multiple dimensions.

II. Investigation of concrete performance based on least squares support vector regression

II. A.Material preparation

The oil palm is a perennial monocotyledonous plant and a tropical woody oil crop, often referred to as the “King of Oils.” China has been cultivating oil palms for over 100 years, with the crop now primarily distributed in Hainan, Yunnan, Guangdong, and Guangxi provinces. During the refining of palm oil, a significant amount of oil palm fruit is consumed, and large quantities of waste materials such as fruit shells and pits are produced. These waste materials are often burned as fuel in refineries. The ash resulting from the combustion of oil palm shells and kernels is known as oil palm shell ash. This material, rich in amorphous SiO_2 glass, possesses high reactivity and holds promise as another mineral admixture for the production of green high-performance concrete. In this study, the ash residue from the combustion of oil palm shells (referred to as raw oil palm shell ash) was subjected to special treatment to reduce its carbon content and increase its fineness, resulting in ultra-fine oil palm shell ash (abbreviated as POFA).

POFA was then used as an auxiliary cementitious material in the preparation of green high-performance concrete, providing theoretical support for the subsequent research work.

II. A. 1) Preparation process and basic properties of POFA

First, the raw oil palm shell ash is dried at a temperature of (100±9)°C until a constant weight is achieved, then sieved through a square mesh screen with a pore size of 0.23 mm to remove coarse particles and non-combustible impurities. Then, grind the material using a ball mill to ensure thorough calcination. Subsequently, calcine the ground oil palm shell ash at a temperature of (100±9)°C for 120 minutes to remove free carbon components that may affect the activity of volcanic ash. Finally, the calcined oil palm shell ash is ground again to obtain POFA for the preparation of green high-performance concrete. The chemical compositions of POFA and OPC are shown in Table 1, where OPC represents ordinary Portland cement. The bulk density is 1673 m/kg, the density is 2.48 g/cm³, and the average particle size is 2.05 μm. The chemical composition of POFA is listed in Table 1, and the specific surface area of POFA is 2.05 μm.

Table 1: The chemical composition of POFA and OPC

Ingredients	SiO_2	Al_2O_3	Fe_2O_3	CaO	MgO	SO_3	Na_2O	LOI	Others
POFA	60.27	6.36	4.79	8.14	5.28	0.74	0.14	2.58	10.64
OPC	21.16	5.02	2.66	57.21	0.76	3.58	1.06	1.58	6.17

II. A. 2) Concrete Constituents and Mix Proportions

The raw materials used to prepare green high-performance concrete were selected in accordance with the relevant provisions of the “Technical Regulations for the Application of High-Strength Concrete.” The cement used is P•O43 grade ordinary Portland cement. The fine aggregate is ordinary river sand with a fineness modulus of 3.05 and an apparent density of 2.58 g/cm³. The coarse aggregate is granite-type crushed stone with a maximum nominal particle size of 27 mm and an apparent density of 2.65 g/cm³. The high-efficiency water-reducing agent is a polycarboxylic acid-based liquid agent. The mix proportions of the five concrete mixtures are shown in Table 2. The water-cement ratio (0.3), total cementitious material content (555 kg/m³), coarse and fine aggregate quantities, and high-efficiency water-reducing agent dosage are all fixed and unchanged for all concrete mixtures. The only variable is the replacement rate (dosage) of POFA. Based on the principle of equal replacement, compared to the reference mix design (designated as CTRL, without POFA), the POFA replacement rates were set at 25%, 50%, and 75% (corresponding mix design designations are POFA25, POFA50, and POFA75). The aforementioned mix design principles were established to clearly examine the effects of adding or not adding POFA and the dosage on concrete performance without interference from other variables.

Table 2: The mix proportion of concrete

Mix proportion code	Unit consumption of raw materials (kg/m³)					
	POFA	OPC	River sand	Crushed stone	Water	High-efficiency water-reducing agent
CTRL	0	555	716	1000	150	11.6
POFA25	100	416	716	1000	150	11.6
POFA50	200	312	716	1000	150	11.6
POFA75	300	208	716	1000	150	11.6
POFA50-2	200	312	716	1000	150	11.6
Remarks: In addition to the above mix ratio, POFA50-2 also contains 6.5% (26.5 kg/m³) of nano calcium carbonate by the total weight of the cementitious materials						

II. A. 3) Specific preparation process

A forced-action mixer is used to mix the concrete. First, crushed stone, river sand, and cement are added to the pre-moistened mixing drum, and dry mixed for 5 minutes. Then, the mixing water, which has been pre-mixed with a high-efficiency water-reducing agent, is evenly poured into the mixing drum, and mixed for 4 minutes. After a 1-minute pause, mixing continues for another 5 minutes before the mixture is discharged and set aside. This completes the preparation of green concrete using oil palm shell aggregate.

II. B. Concrete Property Prediction Model

II. B. 1) Least Squares Support Vector Regression

In the SVR algorithm, solving constrained convex quadratic optimization problems can result in excessively long training times when the sample set is large, leading to low model efficiency. To address this issue, the Least Squares Support Vector Regression (LSSVR) algorithm was proposed. Which is an improvement over the standard SVR algorithm. This algorithm retains all the advantages of the SVR algorithm while further replacing inequality constraints with equality constraints. It uses the squared error loss function of the least squares linear system as the empirical loss for the training set and replaces the solution of the convex quadratic programming problem in the standard SVR algorithm with the solution of the linear equations, significantly reducing computational complexity and improving convergence accuracy, while also demonstrating good generalization performance [40], [41]. The equation for the least squares support vector regression machine is shown in Formula (1):

$$\min J(\omega,\xi)=\frac{1}{2}\omega^T\omega+\frac{\gamma}{2}\sum_{i=1}^{l}\xi^T\xi \tag{1}$$

$$s.t.\quad y_i=\omega^T\varphi(x_i)+b+\xi_i\quad i=1,2,\cdots,l \tag{2}$$

In the equation, $\omega=(\omega_1,\omega_2,\cdots,\omega_l)$ is the weight vector. x_i and y_i are the input and output vectors of the model, respectively. γ is called the regularization parameter, which is used to adjust the severity of error punishment. ξ_i is the slack variable, and b is the bias term. $\varphi(\cdot)$ is a nonlinear mapping function that maps the sample set from a low-dimensional feature space to a high-dimensional feature space. To solve the optimization problem in equation (2), the Lagrange function is introduced, resulting in:

$$L(\omega,b,\xi,\alpha)=J(\omega,\zeta)-\sum_{i=1}^{l}\alpha_i[\omega^T\cdot\varphi(x_i)+b+\xi_i-y_i],i=1,2,\cdots,l \tag{3}$$

In the equation, $\alpha=[\alpha_1,\alpha_2,\cdots,\alpha_l]^T$ is called the Lagrange multiplier. Taking the first-order partial derivatives with respect to ω,b,ξ_i, and α_i, and setting them equal to 0, we obtain the linear system of equations shown in equation (4):

$$\begin{cases}\dfrac{\partial L}{\partial\omega}=0\Rightarrow\omega=\sum_{i=1}^{l}\alpha_i\varphi(x_i)\\ \dfrac{\partial L}{\partial b}=0\Rightarrow\sum_{i=1}^{l}\alpha_i=0\\ \dfrac{\partial L}{\partial\xi_i}=0\Rightarrow\alpha_i=\gamma\xi_i\\ \dfrac{\partial L}{\partial\alpha_i}=0\Rightarrow\omega^T\cdot\varphi(x_i)+b+\xi_i-y_i=0\end{cases} \tag{4}$$

Eliminating the variables ω and ξ_i from equation (4) yields the linear equation system shown in equation (5):

$$\begin{bmatrix}0 & I^T\\ I & \Omega+\gamma^{-1}E\end{bmatrix}\cdot\begin{bmatrix}b\\ \alpha\end{bmatrix}=\begin{bmatrix}0\\ Y\end{bmatrix} \tag{5}$$

In equation (5), $I=[1,1,\ldots,1]^T$ and E are l rd-order unit matrices, $\alpha=[\alpha_1,\alpha_2,\ldots,\alpha_n]^T$ is the Lagrange multiplier, output vectors $Y=[y_1,y_2,\cdots,y_i]^T$ and Ω are kernel functions, and $\Omega_{ij}=\varphi(x_i)\cdot\varphi(x_j)=K(x_i,x_j)$. From equation (5), the estimated values of α and b can be obtained as shown in equation (6). They are:

$$\begin{cases}\hat{\alpha}=\dfrac{Y-bI}{\Omega+\gamma^{-1}E}\\ \hat{b}=\dfrac{I^T(\Omega+\gamma^{-1}E)Y}{I^T(\Omega+\gamma^{-1}E)I}\end{cases} \tag{6}$$

From this, the mathematical model of LSSVR can be derived as shown in Equation (7). It is:

$$\hat{y}=f(x)=\sum_{i=1}^{i}\hat{\alpha}_iK(x_i,x)+\hat{b} \tag{7}$$

Regarding the selection of kernel functions for the LSSVR model, there is currently no unified standard in the academic community. Many studies have shown that different kernel functions can significantly impact the performance of the LSSVR model. In practical applications, the RBF radial basis function is widely used because

its expression is relatively simple and it has radial symmetry, with good analyticity and smoothness. Therefore, this paper first investigates the use of the RBF kernel function to establish the LSSVR model, and then explores the use of multiple kernel functions to improve the model and further enhance its performance.

As can be seen from the above formula, the LSSVR modeling process involves the regularization parameter γ and the RBF kernel function parameter σ. Research results from many scholars indicate that different combinations of parameters γ and σ will significantly affect the fitting accuracy and generalization ability of the LSSVR model, mainly manifested as follows:

(1) The complexity of the LSSVR model and the severity of the penalty for estimation errors are both determined by the regularization parameter γ. When the regularization parameter γ is set to a small value, the model's penalty for fitting error is relatively lenient, leading to increased training and testing errors, resulting in “underfitting” of the LSSVR model: When the regularization parameter γ is set to a large value, the model's penalty for fitting error is relatively stringent, which maximizes the model's ability to satisfy each sample point. This results in a smaller training error but a larger testing error, and the testing error increases as γ increases, leading to “overfitting” of the LSSVR model and poor generalization ability.

(2) The coverage width parameter σ of the RBF radial basis kernel function has a significant impact on the complexity of the final solution. The parameter σ reflects the structure of the high-dimensional feature space $\varphi(x)$, and its value also affects the generalization ability of the LSSVR model. When the value of the parameter σ is small, the model's training error is small while the test error is large, leading to the “overfitting” problem of the LSSVR model. When the value of the parameter σ is large, both the training and test errors of the model are large, leading to the “underfitting” problem of the LSSVR model.

II. B. 2) Gray Wolf Algorithm

The gray wolf algorithm has the advantages of fast convergence speed, global optimization, few parameters, easy implementation, and good robustness, which improves the calculation accuracy of the function optimization, and the principle of the gray wolf algorithm is shown in Figure 1. Gray wolves rely on a strict hierarchy within the pack to complete the hunting and predation process, and a pyramid model is established based on the social hierarchy of the wolf pack, which is divided into four grades from top to bottom: α, β, δ and ω. The hunt is dominated by wolf α, and the gray wolf pack rounds the prey from all directions, and under the leadership of the head wolf α, the β, δ closest to the prey carries out the action, and the remaining wolf pack ω fills the gap to prevent the prey from escaping. The wolves attacked repeatedly and repeatedly, gradually narrowing the encirclement and eventually capturing the prey. Therefore, for all optimization problems, it is the problem of using the GWO algorithm to solve the best coordinates of the prey.

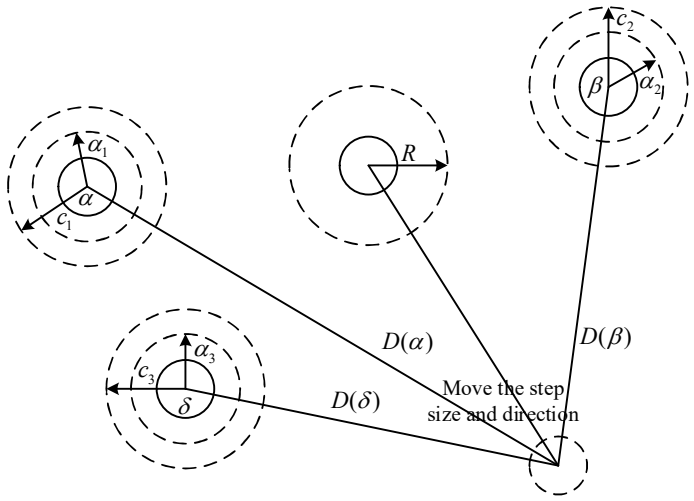

Figure 1: The principle of the Grey Wolf Algorithm

The process by which a wolf pack surrounds its prey is shown in the following equation:

$$D = | CX_p(t) - X(t) | \tag{8}$$

$$X(t+1) = X_p(t) - AD \tag{9}$$

$$C = 2r_1 \tag{10}$$

$$A = a(2r_2 - 1) \tag{11}$$

In the equation: C is the oscillation factor, A is the convergence factor, $X_p(t), X(t)$ are the positions of the prey and gray wolf after the t th iteration, respectively, $r_1 = rand(0,1), r_2 = rand(0,1)$. The GWO algorithm uses the optimal solution of the wolf pack α, β, δ to obtain the potential prey position, enabling other wolf packs to update their hunting positions. This process of surrounding and capturing prey is described by the following mathematical formula.

$$\begin{aligned} D_a &= |C_1 X_a(t) - X(t)| \\ D_\beta &= |C_2 X_\beta(t) - X(t)| \\ D_\delta &= |C_3 X_\delta(t) - X(t)| \\ X_1 &= X_s(t) - A_1 D_s \\ X_2 &= X_\beta(t) - A_2 D_\beta \\ X_3 &= X_3(t) - A_3 D_3 \end{aligned} \tag{12}$$

Calculate the new position of individuals within the population after iteration according to the following formula:

$$X(t+1) = \frac{(X_1 + X_2 + X_3)}{3} \tag{13}$$

II. B. 3) DE-GWO Algorithm

The GWO algorithm can only alleviate local optima to a certain extent. Therefore, a method based on global optimization, the differential evolution algorithm, is introduced. This method updates the population through mutation, crossover, and selection operations on individuals with different differences in the population to obtain the global optimal solution. In D-dimensional space, POP represents the population, with the following definitions:

$$\begin{aligned} POP &= \{X^1, X^2, \cdots, X^k, \cdots, X^{psize}\} \\ X^k &= (X_1^k, X_2^k, \cdots, X_p^k, \cdots, X_d^k) \end{aligned} \tag{14}$$

k denotes the k th individual, $k = 1, 2, \cdots, psize$, where $psize$ denotes the size of the sample population, $p = 1, 2, \cdots, d$.

(1) Randomly generate the initial population in the search space:

$$X_p^k = X_p^k(\text{low}) + (X_p^k(\text{up}) - X_p^k(\text{low})) \times \text{rand}(0,1) \tag{15}$$

$X_p^k(\text{low})$ represents the lower bound of the p th component of the k th individual, $X_P^K(\text{up})$ represents the upper bound of the p th component of the k th individual, and rand(0, 1) represents a random number between [0, 1].

(2) Mutation operation

Mutation individuals are generated by the following equation:

$$V^i(\tau) = X^{r_1}(\tau) + M \cdot (X^{r_2}(\tau) - X^{r_3}(\tau)) \tag{16}$$

In the formula, M is the scaling factor, $r_1 \neq r_2 \neq r_3 \neq i$. $\tau = 0, 1, 2, \cdots, \tau_{\max}$ represents the number of iterations.

(3) Cross operation:

$$U_j^k(\tau) = \begin{cases} V_j^k(\tau), \text{rand}(0,1) \leq CR \text{ or } j = \text{rand}(1,d) \\ X_j^k(\tau), \text{rand}(0,1) > CR \text{ or } j \neq \text{rand}(1,d) \end{cases} \tag{17}$$

In the formula: CR is the crossover probability factor, $rand(1,d)$ is a random integer between $[1,d]$, and d is the sample dimension.

(4) Selection operation

Ensure the superiority of the offspring population:

$$X^k(\tau+1) = \begin{cases} X^k(\tau), f(U^k(\tau)) > f(X^k(\tau)) \\ U^k(\tau), f(U^k(\tau)) \leq f(X^k(\tau)) \end{cases} \tag{18}$$

Although the GWO algorithm demonstrates its superiority in many fields, like other intelligent algorithms, it is prone to local optima, slow computation speeds, and reduced accuracy when training objects are large data samples. Therefore, this paper uses the differential algorithm to update the optimal position of the wolf pack to avoid the GWO algorithm falling into local optima.

II. B. 4) Modeling steps for the DE-GWO-LSSVR combination model

The DE-GWO-LSSVR model was used to predict the performance of green concrete made from oil palm shell aggregate. The model construction process consists of two stages. Stage one is the preliminary data preparation stage for the model, with the following steps:

(1) Data cleaning stage. This stage primarily involves processing missing and outlier data in the collected oil palm shell aggregate green concrete data. The primary method used in this stage is spline interpolation, which corrects missing and outlier data by using the average of the sample data before and after the missing or outlier data point.

(2) Feature construction stage. This stage involves conducting correlation analysis on the original features and, based on the original features, further utilizing the hidden information in the data through manual feature construction to obtain better feature combinations for the model training process.

(3) Sample division stage. The entire sample space is divided into training data and test data. The training data is used to establish a mathematical model, and the prediction data is used to evaluate the model's performance.

(4) Training label construction stage. The time difference between the current time of the sample and the detection time is used as the training label, which represents the performance of oil palm shell aggregate green concrete.

(5) Feature data normalization stage. Through data normalization operations, the sample data is scaled to the range [0, 1], which not only accelerates the model's iterative convergence speed but also eliminates the impact of different features with different dimensions on the prediction results. The data normalization function is:

$$x_i^{'} = \frac{x_i - x_{\min}}{x_{\max} - x_{\min} + 0.01} \tag{19}$$

In the formula: $x_i^{'}$ represents the normalized value. x_i represents the unnormalized value. $x_{\max}, x_{\min}$ represent the maximum and minimum values of the data under this feature, respectively. The purpose of adding 0.01 to the denominator of this formula is to prevent the denominator from being 0.

(6) Kernel function selection stage. This paper selects the radial basis kernel function, i.e.:

$$K(x, x_i) = \exp\left[-\frac{\| x - x_i \|^2}{2\sigma^2}\right] \tag{20}$$

In the formula, $\| x - x_i \|$ represents the distance between x and x_i. σ represents the kernel width parameter.

Stage two is the model prediction stage. The prediction steps of the DE-GWO-LSSVR model-based algorithm for predicting the performance of green concrete made from oil palm shell aggregate are shown in Figure 2.

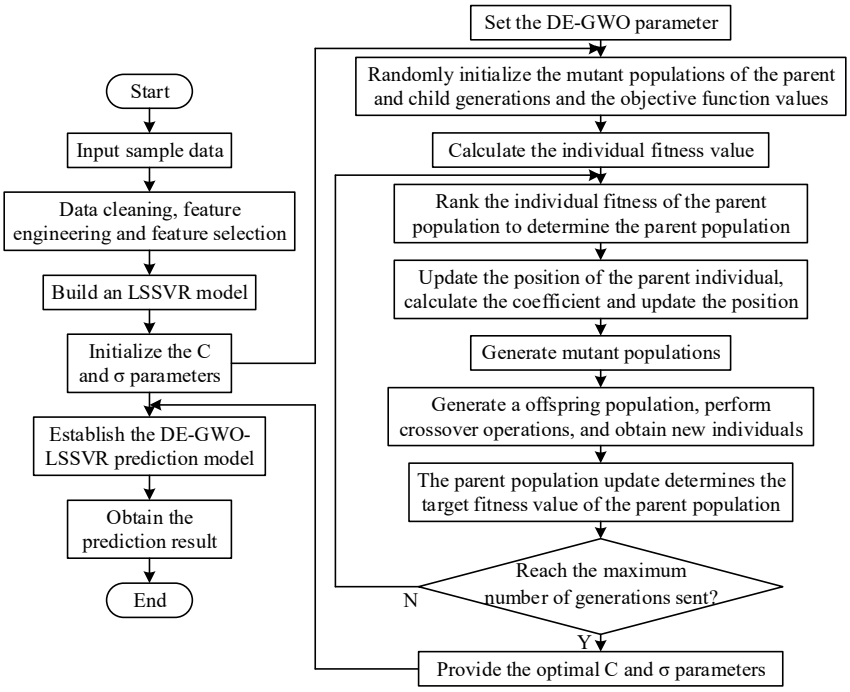

Figure 2: Prediction process

The prediction process is explained as follows:

(1) Initialize the model training parameters.

(2) Initialize the population according to the formula, where the optimization parameters are C and σ, and these two parameters constitute each wolf pack individual X.

(3) Calculate the fitness value of each individual and sort the individuals in ascending order of fitness value. Select the top three individuals X_α, X_β and X_δ as the upper-level wolves.

(4) Use the differential algorithm to update the positions of the parent-generation wolves.

(5) Apply mutation and crossover operations to the wolf pack using the formula to obtain the new offspring wolf pack.

(6) Use the formula selection operation to select the optimal parent population and update A, C according to the formula.

(7) Continuously iterate and update the population until the termination condition is met. At this point, the value of the optimal position of the wolf in the obtained parent population is the optimal parameter C, σ.

(8) Construct the LSSVR model based on the optimal parameters.

III. Empirical Research Analysis

III. A. Dataset

III. A. 1) Obtaining Data

Before conducting empirical research, it is necessary to first create a dataset. Although many researchers have used machine learning algorithms to predict the strength of oil palm shell aggregate green concrete, no studies have yet been conducted to construct a public dataset. Therefore, this paper requires a dataset composed of test data on oil palm shell aggregate green concrete in order to develop a model for predicting the performance of oil palm shell aggregate green concrete. The construction of the dataset must fully consider data collection and preprocessing methods to ensure data accuracy and reliability. For dataset construction, appropriate features and labels must be selected to ensure sufficient sample size and uniform data distribution. This paper obtained data from other studies on oil palm shell aggregate green concrete based on machine learning algorithms. The dataset consists of 6 input features and 1 output target (DIF refers to the ratio of compressive strength under dynamic load to compressive strength under quasi-static load). Table 3 presents the descriptive statistics of the study data. The results show that the minimum value of POFA is 100, the maximum value is 300, the mean is 253, and the standard deviation is 12.3. The remaining five input features and one output target are as shown in the table and will not be described in detail here.

Table 3: Descriptive statistics of data

Feature	Quantity	Average value	Standard deviation	Min	Max
POFA	100	253	12.3	100	300
OPC	100	361	22.3	200	600
River sand	100	692	31.7	100	800
Crushed stone	100	839	50.5	500	1000
Water	100	130	10.6	100	150
High-efficiency water-reducing agent	100	11.3	1.8	10	15
DIF	100	1.9	0.6	0.8	3.6

Figure 3 shows the variable relationship diagram of the DIF dataset. In the figure, X1 to X6 represent POFA, OPC, river sand, crushed stone, water, and high-efficiency water-reducing agent, respectively. As can be seen from the figure, DIF increases with increases in POFA, OPC, river sand, and water, while an increase in crushed stone reduces DIF. The effect of high-efficiency water-reducing agent on DIF is not significant.

Figure 4 shows the feature correlation coefficient matrix, and similar results can be obtained from the correlation coefficient matrix in Figure 3. POFA, OPC, river sand, and water exhibit positive correlations with DIF, with correlation coefficients of 0.427, 0.535, 0.494, and 0.477, respectively. Crushed stone and high-efficiency water-reducing agent exhibit negative correlations, with correlation coefficients of -0.363 and -0.168, respectively.

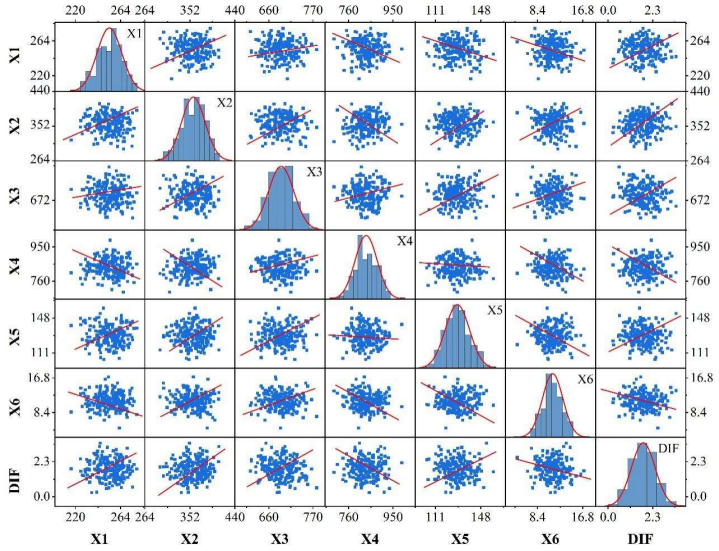

Figure 3: The variable relationship diagram of the DIF dataset

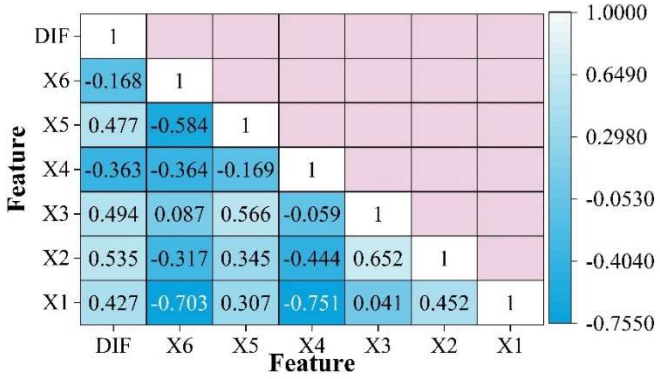

Figure 4: Feature correlation coefficient matrix

III. A. 2) Division of training sets and test sets

One common method for constructing and evaluating the performance of machine learning models is to divide the dataset into a training set and a test set. The training set is used to fit and train the model, while the test set is used to evaluate the performance of the trained model on new data, thereby assessing the model's generalization ability. In modeling, to avoid overfitting and improve the robustness of the model, the dataset is typically split into a training set and a test set according to a certain ratio (e.g., 7:3, 8:2, etc.). In this paper, the train test split function in Sklearn is used to randomly split the dataset into a training set and a test set according to a 7:3 ratio, ensuring that the distribution differences between the training set and the test set are as small as possible and reducing the risk of overfitting to certain data. Then, using the training set data, four models—LSSVR, RF, GBDT, and XGBoost—were established, with the composition components of oil palm shell aggregate green concrete (POFA, OPC, river sand, crushed stone, water, and high-efficiency water-reducing agent) as input features and DIF as the output result, to establish the correlation between the mix ratio, test parameters, and the DIF of oil palm shell aggregate green concrete. Using the improved gray wolf algorithm, the hyperparameters of the prediction models are adjusted to achieve the best fitting effect, ensuring that each model's predictive capability reaches its optimal performance.

III. B. Analysis of the optimization effect of the DE-GWO algorithm

III. B. 1) Experimental setup

From the computational steps of the four methods—Genetic Algorithm (GA), Particle Swarm Optimization (PSO), Cuckoo Search (CS), and Improved Gray Wolf Optimization (DE-GWO)—each optimization method uses a biological population as a model to calculate the solution set. Each individual in the population represents a solution to the model. The population is randomly generated, forming the solution set. The population size is manually set, and then the optimal solution is sought based on the characteristics and behaviors of the biological entities. Among these, the Genetic Algorithm (GA) converges faster than other algorithms and has strong global search capabilities.

However, during iterative calculations, it may tend to “mature too early,” resulting in suboptimal solutions rather than the optimal solution. The Particle Swarm Optimization (PSO) algorithm has weak search capabilities in the later stages of iteration and insufficient search precision. The cuckoo search algorithm (CS) converges slowly. The improved gray wolf algorithm (DE-GWO) uses a combination of solutions to find the optimal solution more reasonably. Combining the four algorithms with the least squares support vector regression model (LSSVR) for optimization yields the following results.

III. B. 2) Analysis of Results

The prediction results of different optimization models are shown in Figure 5, where (a) to (d) represent GA-LSSVR, PSO-LSSVR, CS-LSSVR, and DE-GWO-LSSVR, respectively. The results show that compared to the LSSVR model with hyperparameters selected via cross-validation, the optimized models exhibit increased prediction correlation coefficients and reduced prediction root mean square errors, indicating effective optimization. This suggests that utilizing intelligent swarm algorithms for parameter optimization enhances the accuracy of the least squares support vector regression model. Among them, the optimized prediction correlation coefficient based on the GA algorithm is 0.99421, and the prediction root mean square error is 0.423%. Compared with the other three optimization methods, although its computation time is the shortest, the improvement in prediction performance is the smallest. This is because the memory-free nature of the GA algorithm causes information loss in the solution vector, resulting in weaker optimization effects. The other three optimization methods, however, preserve the corresponding information when obtaining good solution vectors. The correlation coefficient of the optimization prediction based on the PSO algorithm is lower than that of the optimization prediction based on the CS algorithm, resulting in relatively poorer prediction performance. However, its prediction root mean square error is smaller than that of the latter, indicating that the optimization model based on the PSO algorithm has better stability. The root mean square error of the optimization prediction based on the PSO algorithm is the same as that of the optimization prediction based on the DE-GWO algorithm, but the correlation coefficient of the latter is larger than that of the former. This is because the PSO algorithm may exhibit premature convergence and incomplete optimization during parameter selection, resulting in the obtained optimal solution not being the global optimal solution. The optimization prediction based on the DE-GWO algorithm has the largest correlation coefficient and the smallest root mean square error, making it the best in terms of prediction performance among the four methods.

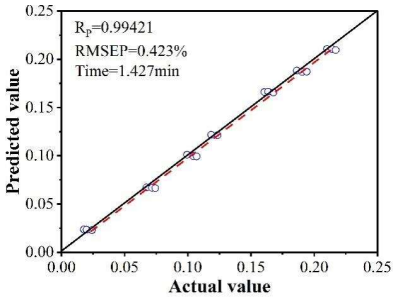

(a)GA-LSSVR

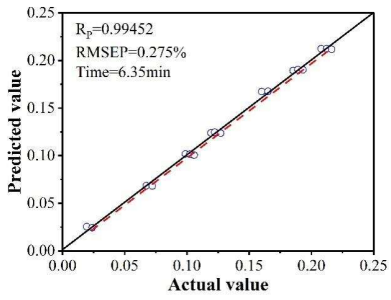

(b)PSO-LSSVR

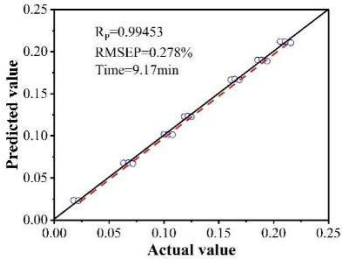

(c)CS-LSSVR

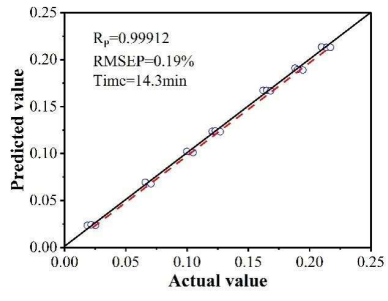

(d)DE-GWO-LSSVR

Figure 5: Prediction results of different optimization models

III. C. Model Evaluation Analysis

III. C. 1) Evaluation Indicators

Model evaluation refers to the process of assessing and verifying the performance of a model. Its purpose is to determine the effectiveness and reliability of the model in specific tasks. Model evaluation metrics provide performance measurements from different perspectives, enabling a comprehensive understanding of the model's performance capabilities. Common model evaluation metrics include:

$$RMSE = \sqrt{\frac{1}{n}\sum_{i=1}^{n}(T-Y)^2} \tag{21}$$

$$MAE = \frac{1}{n}\sum_{i=1}^{n}(T-Y) \tag{22}$$

$$MSE = \frac{1}{n}\sum_{i=1}^{n}(T-Y)^2 \tag{23}$$

$$R^2 = 1-\frac{\sum_{i=1}^{n}(T-Y)^2}{\sum_{i=1}^{n}(T-\overline{Y})^2} \tag{24}$$

$$MAPE = \frac{1}{n}\sum_{i=1}^{n}\left|\frac{T_i-Y_i}{T_i}\right|\times 100\% \tag{25}$$

Among them, T and Y represent the experimental results and predicted results, respectively, and $\overline{T}$ is the average value of $\overline{Y}$.

III. C. 2) Data Analysis

The dataset was divided into two parts in a 7:3 ratio, with 70% of the data used to train the RF, GBDT, XGBoost, and DE-GWO-LSSVR models, thereby obtaining a predictive model for the performance of green concrete made from oil palm shell aggregate. The remaining 30% of the test set data was used to evaluate the model's performance using four assessment metrics. By comparing the performance of the DE-GWO-LSSVR model with that of the three classical prediction models on the test set, the application effectiveness of the DE-GWO-LSSVR model in predicting the performance of oil palm shell aggregate green concrete was analyzed.

The performance metrics of each prediction model are shown in Table 4. The prediction results indicate that, considering the four aspects of RMSE, MSE, MAE, and R^2, the DE-GWO-LSSVR model constructed in this paper exhibits higher prediction accuracy and more stable prediction results, with model prediction metrics RMSE, MSE, MAE, and R^2 being 1.36, 1.97, 1.05, and 0.88, respectively. Figure 6 compares the predicted values and actual values of the four models for the performance of green concrete using oil palm shell aggregate, where (a) to (d) represent the RF, GBDT, XGBoost, and DE-GWO-LSSVR models, respectively. It can be clearly seen that in the test set, all four models provide relatively accurate predictions of the performance of oil palm shell aggregate green concrete. Among them, the DE-GWO-LSSVR model has the highest prediction accuracy, with a correlation coefficient R^2 = 0.88. The RF model has the worst prediction performance, with a correlation coefficient R^2 = 0.47.

Table 4: Comparison of prediction errors of different models

Model	RMSE	MSE	MAE	R^2
RF	2.17	4.94	1.66	0.47
GBDT	2.12	4.18	1.59	0.59
XGBoost	2.06	4.46	1.65	0.58
DE-GWO-LSSVR	1.36	1.97	1.05	0.88

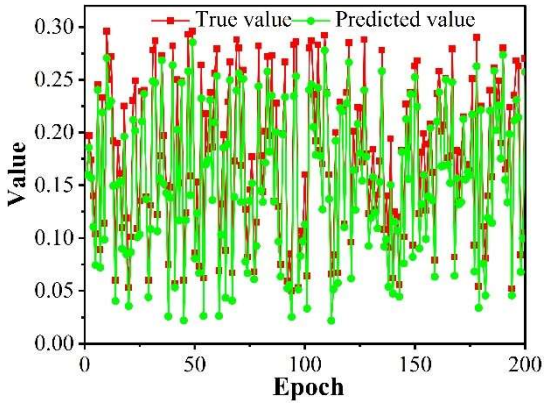

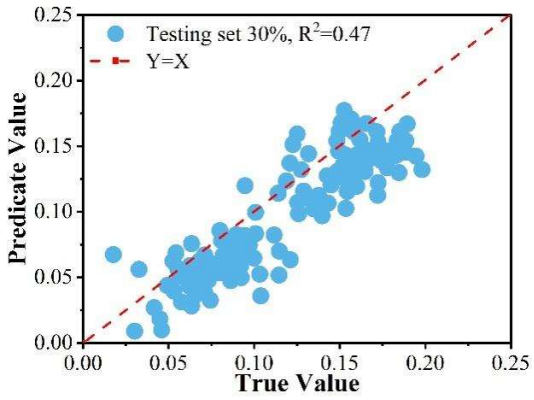

(a) RF

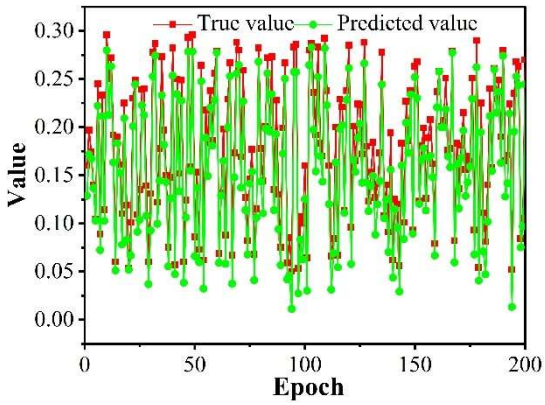

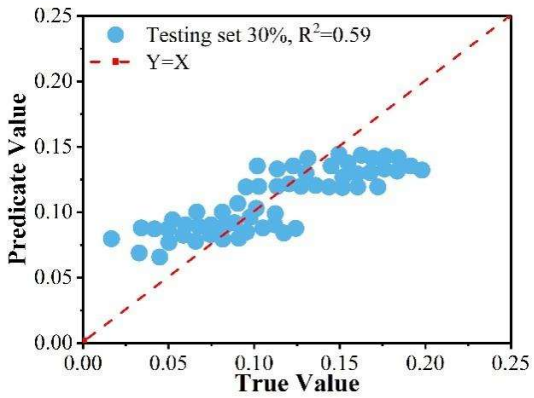

(b) GBDT

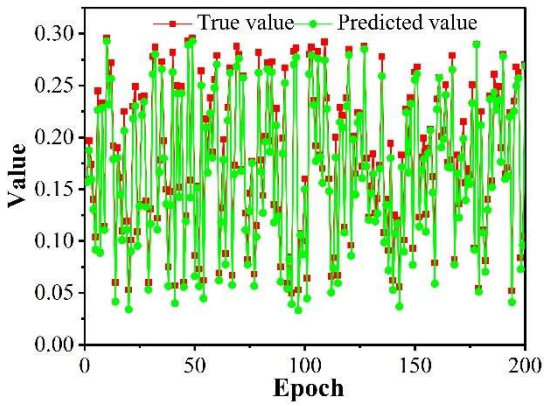

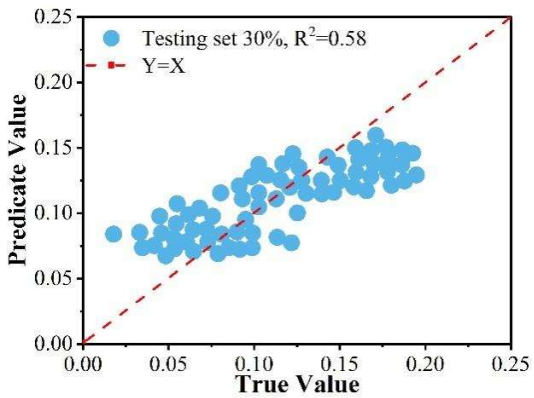

(c) XGBoost

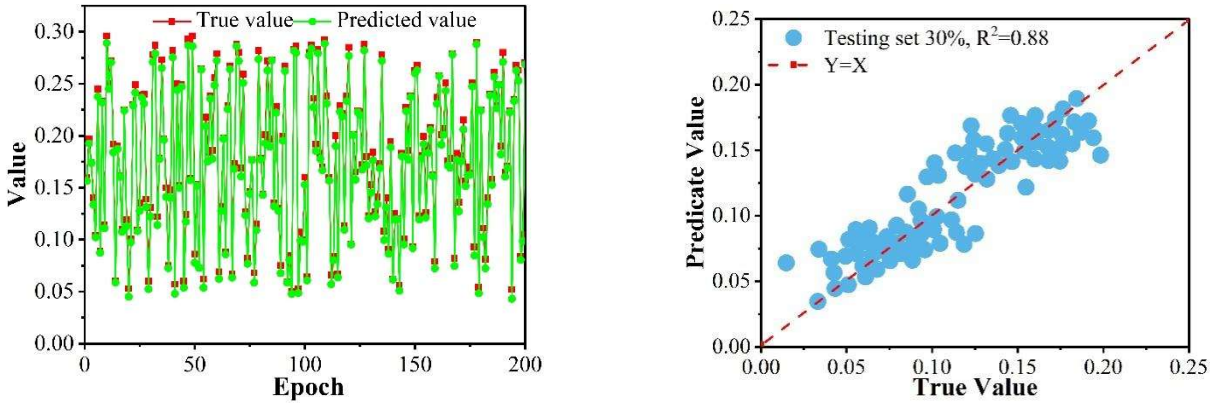

(d) DE-GWO-LSSVR

Figure 6: Comparison of prediction results

III. D. Interpretability and reverse optimization design analysis

III. D. 1) Interpretability Analysis

This section investigates the influence of feature parameters on the performance of green concrete made from oil palm shell aggregate and employs a DE-GWO-LSSVR model-based approach to conduct a model interpretability analysis of FID values. The FID value is a tool used to quantify model interpretability. On one hand, the larger the total FID value of a particular feature, the greater its impact on the overall performance of the model. On the other hand, for a specific feature and each classification label, a larger FID value indicates that the feature is more important for predicting the corresponding label, thereby increasing the likelihood of correctly predicting that label. The importance analysis of each feature is shown in Figure 7, where (a) and (b) represent the FID feature importance and FID value scatter plot, respectively. From the figure, it can be seen that for this dataset, the most important input feature variables are POFA, OPC, river sand, crushed stone, water, and high-efficiency water-reducing agent, among which POFA has the most significant impact on the performance of oil palm shell aggregate green concrete.

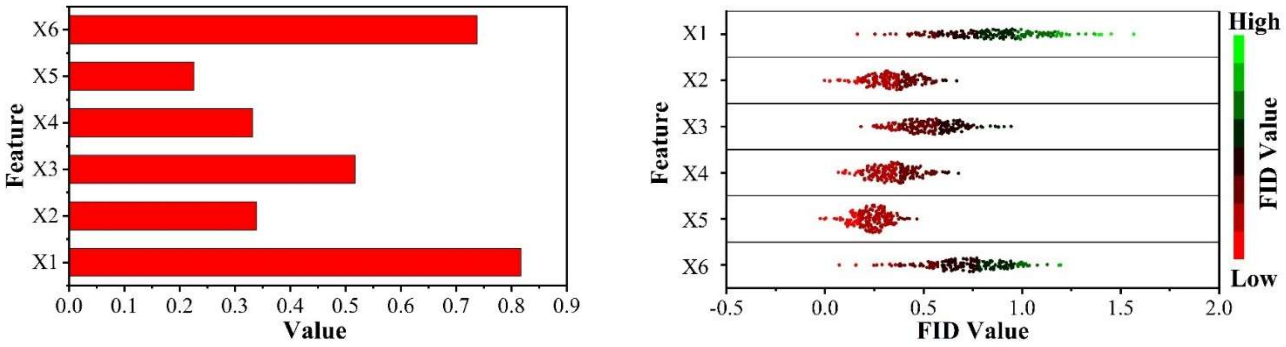

(a) The importance of FID features

(b) Scatter plot of FID values

Figure 7: Interpretability analysis

III. D. 2) Reverse Optimization Design Analysis

The raw materials used for preparing green concrete with oil palm shell aggregate—POFA, OPC, river sand, crushed stone, water, and high-efficiency water-reducing agent—are supplied by International Engineering Co., Ltd. The chemical composition is shown in Table 5. The raw materials were ground into powder, mixed with 8% gypsum in a mixer until uniform, then mixed with 3.5% deionized water. The mixture was pressed at 25 MPa pressure for 50 seconds to form circular specimens measuring 300 mm × 20 mm, which were then dried in a 120°C oven for 24 hours. First, the oil palm shell aggregate green concrete samples were calcined at 500°C in a muffle furnace for 1 hour, then quickly transferred to a high-temperature furnace at 1800°C for calcination and insulation for 1 hour. After calcination, the samples were directly removed and rapidly cooled to room temperature. A vibrating mill was used

to grind the specific surface area to within (400±50) m²/kg. The f-CaO content in the sample was determined using the ethylene glycol-ethanol method, and the results are shown in Table 6. According to “Oil Palm Shell Aggregate Green Concrete Performance Test Method,” oil palm shell aggregate green concrete test blocks were prepared and tested for strength.

Table 5: Chemical composition(%)

Oxides	X1	X2	X3	X4	X5	X6
SiO_2	4.274	28.352	41.756	4.216	2.643	18.759
Al_2O_3	1.183	22.071	44.307	6.29	2.51	23.639
Fe_2O_3	4.487	18.486	41.068	4.169	2.187	29.603
CaO	4.609	29.168	44.74	4.212	3.212	14.059
MgO	0.613	20.366	44.49	7.449	2.958	24.124
SO_3	0.542	23.052	45.358	5.672	3.497	21.879
Na_2O	4.537	15.563	48.88	4.087	2.079	24.854
LOI	4.568	18.799	42.61	6.627	2.861	24.535
Others	1.197	25.947	40.596	6.145	2.086	24.029

Table 6: The f-CaO content of the sample (%)

Sample	CTRL	POFA25	POFA50	POFA75	POFA50-2
f-CaO	0.54	0.62	0.64	0.67	0.71

This section uses the output results of the DE-GWO-LSSVR model to set the optimization objective (the compressive strength of the five test samples should be distributed between 60.36 and 63.33 MPa within 14 days), combined with the DE-GWO optimization algorithm to adjust the clinker mix ratio. Under the specified constraints, the clinker mix ratio is iteratively optimized until the target clinker strength performance is achieved or convergence to the optimal solution is reached, and the results are validated through experimental verification. Based on this target strength range, the DE-GWO optimization algorithm was used for iterative optimization, yielding five optimal clinker mix designs, as shown in Table 7. These results align with the conventional fluctuation range of oxide compositions in oil palm shell aggregate green concrete. Corresponding raw material ratios were calculated based on these results, as shown in Table 8. Figure 8 displays the compressive strengths of the five samples at 6 days and 14 days. As shown in Figure 8, the actual measured values of the 14-day strength fall within the range [60.42 MPa, 62.72 MPa], with a deviation of less than 1 MPa from the target value range [60.36 MPa, 63.33 MPa]. This indicates that the experimental results are in good agreement with the target strength values, thereby validating the reliability and applicability of the DE-GWO-LSSVR model.

Table 7: The composition of the oxide ratio of clinker for the target strength(%)

Oxides	CTRL	POFA25	POFA50	POFA75	POFA50-2
SiO_2	23.38	23.09	22.22	21.39	20.28
Al_2O_3	4.05	4.28	4.04	4.24	5.86
Fe_2O_3	4.58	4.49	4.16	3.58	5.04
CaO	67.99	68.14	69.58	70.79	68.82

Table 8: Raw materials proportions(%)

Raw materials	CTRL	POFA25	POFA50	POFA75	POFA50-2
POFA	66.31	42.37	16.28	11.45	16.13
OPC	9.84	8.46	9.58	5.27	3.16
River sand	3.46	5.06	4.18	3.44	9.77
Crushed stone	5.86	5.79	3.94	1.09	6.86
Water	14.53	13.32	16.02	3.75	14.08
High-efficiency water-reducing agent	66.31	42.37	16.28	11.45	16.13

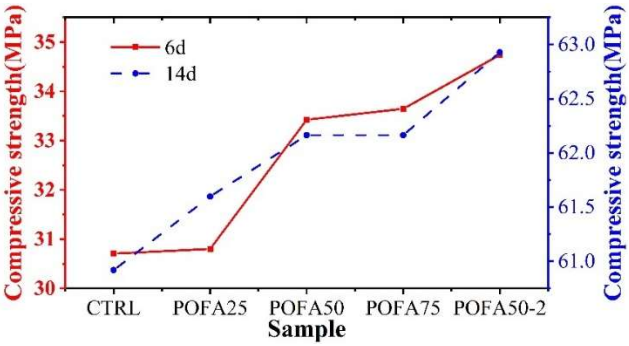

Figure 8: Compressive strength test

IV. Conclusion

This paper first defines oil palm shell aggregate green concrete and prepares five samples of oil palm shell aggregate green concrete based on the corresponding material mix ratios and preparation processes. Addressing the limitations of the least squares support vector regression (LSSVR) model in predicting the performance of oil palm shell aggregate green concrete, this study proposes optimizing the LSSVR model using the differential-grey wolf optimization (DE-GWO) algorithm. Ultimately, a performance prediction model for oil palm shell aggregate green concrete based on DE-GWO-LSSVR is designed. Under the support of the research dataset, an empirical analysis of the performance prediction model for oil palm shell aggregate green concrete was conducted. The data showed that the actual measured values of the 14-day strength of the five oil palm shell aggregate green concrete samples were distributed within the range of [60.42 MPa, 62.72 MPa], while the set target values were [60.36 MPa, 63.33 MPa]. The deviation between the two was within 1 MPa, fully validating the application effectiveness of the proposed model in predicting the performance of oil palm shell aggregate green concrete.

References

[1] Wasim, M., Abadel, A., Bakar, B. A., & Alshaikh, I. M. (2022). Future directions for the application of zero carbon concrete in civil engineering–A review. Case Studies in Construction Materials, 17, e01318.

[2] Teh, S. H., Wiedmann, T., Castel, A., & de Burgh, J. (2017). Hybrid life cycle assessment of greenhouse gas emissions from cement, concrete and geopolymer concrete in Australia. Journal of cleaner production, 152, 312-320.

[3] Habert, G., Miller, S. A., John, V. M., Provis, J. L., Favier, A., Horvath, A., & Scrivener, K. L. (2020). Environmental impacts and decarbonization strategies in the cement and concrete industries. Nature Reviews Earth & Environment, 1(11), 559-573.

[4] Sandanayake, M., Gunasekara, C., Law, D., Zhang, G., Setunge, S., & Wanijuru, D. (2020). Sustainable criterion selection framework for green building materials–An optimisation based study of fly-ash Geopolymer concrete. Sustainable Materials and Technologies, 25, e00178.

[5] Assi, L., Carter, K., Deaver, E. E., Anay, R., & Ziehl, P. (2018). Sustainable concrete: Building a greener future. Journal of cleaner production, 198, 1641-1651.

[6] Sivakrishna, A., Adesina, A., Awoyera, P. O., & Kumar, K. R. (2020). Green concrete: A review of recent developments. Materials Today: Proceedings, 27, 54-58.

[7] Antony, M. R., Rajendran, R. R., Al-Khazaleh, M., & Joe, A. (2023). Thermal insulation performance of green concrete using bio and industrial wastes: An experimental approach. Materials Today: Proceedings.

[8] Hashmi, A. F., Khan, M. S., Bilal, M., Shariq, M., & Baqi, A. (2022). Green concrete: an eco-friendly alternative to the OPC concrete. Construction, 2(2), 93-103.

[9] Alhazmi, H., Shah, S. A. R., & Basheer, M. A. (2021). Performance evaluation of road pavement green concrete: An application of advance decision-making approach before life cycle assessment. Coatings, 11(1), 74.

[10] Huynh, T. P., Hwang, C. L., & Limongan, A. H. (2018). The long-term creep and shrinkage behaviors of green concrete designed for bridge girder using a densified mixture design algorithm. Cement and Concrete Composites, 87, 79-88.

[11] Al-Mansour, A., Chow, C. L., Feo, L., Penna, R., & Lau, D. (2019). Green concrete: By-products utilization and advanced approaches. Sustainability, 11(19), 5145.

[12] Zhang, L. V., Nehdi, M. L., Suleiman, A. R., Allaf, M. M., Gan, M., Marani, A., & Tuyan, M. (2021). Crack self-healing in bio-green concrete. Composites Part B: Engineering, 227, 109397.

[13] Vishwakarma, V., & Ramachandran, D. (2018). Green Concrete mix using solid waste and nanoparticles as alternatives–A review. Construction and Building Materials, 162, 96-103.

[14] Ramasubramani, R., & Gunasekaran, K. (2021). Sustainable alternate materials for concrete production from renewable source and waste. Sustainability, 13(3), 1204.

[15] Al-Gahtani, K., Alsulaihi, I., Ali, M., & Marzouk, M. (2017). Production of green concrete using recycled waste aggregate and byproducts. Built Environment Project and Asset Management, 7(4), 413-425.

[16] Şanal, İ. (2018). Fresh - state performance design of green concrete mixes with reduced carbon dioxide emissions. Greenhouse Gases: Science and Technology, 8(6), 1134-1145.

[17] Ahdal, A. Q., Amrani, M. A., Ghaleb, A. A., Abadel, A. A., Alghamdi, H., Alamri, M., ... & Shameeri, M. (2022). Mechanical performance and feasibility analysis of green concrete prepared with local natural zeolite and waste PET plastic fibers as cement replacements. Case Studies in Construction Materials, 17, e01256.
[18] Harilal, M., Rathish, V. R., Anandkumar, B., George, R. P., Mohammed, M. H. S., Philip, J., & Amarendra, G. (2019). High performance green concrete (HPGC) with improved strength and chloride ion penetration resistance by synergistic action of fly ash, nanoparticles and corrosion inhibitor. Construction and Building Materials, 198, 299-312.
[19] Alani, A. H., Bunnori, N. M., Noaman, A. T., & Majid, T. A. (2019). Durability performance of a novel ultra-high-performance PET green concrete (UHPPGC). Construction and Building Materials, 209, 395-405.
[20] Oseghale, S. D., Mohamed, A. F., & Chikere, A. O. (2017). Status evaluation of palm oil waste management sustainability in Malaysia. OIDA International Journal of Sustainable Development, 10(12), 41-48.
[21] Okoli, I. C. (2020). Oil Palm Tree Wastes 6: Uses of the palm kernel shell. Tropical Research Reference Platform, 1.
[22] Nasir, S., Hussein, M. Z., Zainal, Z., Yusof, N. A., & Mohd Zobir, S. A. (2018). Electrochemical energy storage potentials of waste biomass: oil palm leaf-and palm kernel shell-derived activated carbons. Energies, 11(12), 3410.
[23] Mushtaq, F., Malghani, M. N. K., Nasar, M. S., Mengal, A. N., Mat, R., & Ani, F. N. (2017). Pyrolysis heating performance of oil palm shell waste biomass with carbon surfaces. Journal of Applied and Emerging Sciences, 7(1), pp70-75.
[24] Yahayu, M., Abas, F. Z., Zulkifli, S. E., & Ani, F. N. (2018). Utilization of oil palm fiber and palm kernel shell in various applications. Sustainable technologies for the management of agricultural wastes, 45-56.
[25] Maghfouri, M., Shafigh, P., & Aslam, M. (2018). Optimum oil palm shell content as coarse aggregate in concrete based on mechanical and durability properties. Advances in Materials Science and Engineering, 2018(1), 4271497.
[26] Kareem, M. A., Raheem, A. A., Oriola, K. O., & Abdulwahab, R. (2022). A review on application of oil palm shell as aggregate in concrete-Towards realising a pollution-free environment and sustainable concrete. Environmental Challenges, 8, 100531.
[27] Traore, Y. B., Messan, A., Hannawi, K., Gerard, J., Prince, W., & Tsobnang, F. (2018). Effect of oil palm shell treatment on the physical and mechanical properties of lightweight concrete. Construction and Building Materials, 161, 452-460.
[28] Rahman, N. A., Tan, A. S. H., Waqbitu, F., & Roslan, N. H. (2020, April). The effectiveness of oil palm shell (OPS) as major aggregate replacement in concrete. In IOP Conference Series: Earth and Environmental Science (Vol. 476, No. 1, p. 012019). IOP Publishing.
[29] Muthusamy, K., Budiea, A. M. A., Azhar, N. W., Jaafar, M. S., Mohsin, S. M. S., Arifin, N. F., & Yahaya, F. M. (2021). Durability properties of oil palm shell lightweight aggregate concrete containing fly ash as partial cement replacement. Materials Today: Proceedings, 41, 56-60.
[30] Han, L. (2024). Green concrete with oil palm shell aggregate: usage of the chaos game-based tree algorithm. Multiscale and Multidisciplinary Modeling, Experiments and Design, 1-18.
[31] Zhu, W., Huang, L., Mao, L., & Esmaeili‐Falak, M. (2022). Predicting the uniaxial compressive strength of oil palm shell lightweight aggregate concrete using artificial intelligence‐based algorithms. Structural Concrete, 23(6), 3631-3650.
[32] Tian, Z. N., Gao, X. X., Xia, T., & Zhang, X. B. (2023). Evaluation of Landweber Coupled Least Square Support Vector Regression Algorithm for Electrical Capacitance Tomography for LN2–VN2 Flow. Energies, 16(22), 7661.
[33] Parand, K., Razzaghi, M., Sahleh, R., & Jani, M. (2022). Least squares support vector regression for solving Volterra integral equations. Engineering with Computers, 38(Suppl 1), 789-796.
[34] Zhu, B., Han, D., Wang, P., Wu, Z., Zhang, T., & Wei, Y. M. (2017). Forecasting carbon price using empirical mode decomposition and evolutionary least squares support vector regression. Applied energy, 191, 521-530.
[35] Ayubi Rad, M., & Ayubirad, M. S. (2017). Comparison of artificial neural network and coupled simulated annealing based least square support vector regression models for prediction of compressive strength of high-performance concrete. Scientia Iranica, 24(2), 487-496.
[36] Zhang, J., & Wang, Y. (2021). Evaluating the bond strength of FRP-to-concrete composite joints using metaheuristic-optimized least-squares support vector regression. Neural Computing and Applications, 33(8), 3621-3635.
[37] Gholampour, A., Mansouri, I., Kisi, O., & Ozbakkaloglu, T. (2020). Evaluation of mechanical properties of concretes containing coarse recycled concrete aggregates using multivariate adaptive regression splines (MARS), M5 model tree (M5Tree), and least squares support vector regression (LSSVR) models. Neural Computing and Applications, 32, 295-308.
[38] Wang, Y., Chen, L., Wang, N., Gu, J., & Wang, Z. (2020). Three-dimensional acoustic emission source localisation in concrete based on sparse least-squares support vector regression. Insight-Non-Destructive Testing and Condition Monitoring, 62(8), 471-477.
[39] Islam, M., & Afrin, S. (2024). Usage of Optimized Least Square SVR to Volume Expansion Estimation of Cement Paste Including Fly Ash and Mgo Expansive Additive. Advances in Engineering and Intelligence Systems, 3(03), 53-68.
[40] Pu Zhou & Yin Lunyu. (2024). A comparative study of LSSVR analysis on ground granulated blast-furnace slag-based concrete. Multiscale and Multidisciplinary Modeling, Experiments and Design,8(1),79-79.
[41] Nhat-Duc Hoang,Xuan-Linh Tran & Hieu Nguyen. (2019). Predicting ultimate bond strength of corroded reinforcement and surrounding concrete using a metaheuristic optimized least squares support vector regression model. Neural Computing and Applications,32(11),1-21.